Int. J. Multiphase Flow Vol. 13, No. 4, pp. 477–491, 1987
Printed in Great Britain.

0301-9322/87 $3.00 + 0.00

BUBBLE BEHAVIOR IN A THREE-PHASE FLUIDIZED BED

D. A. PETERSON,[1]† R. S. TANKIN[2] and S. G. BANKOFF[1,2]‡

Departments of [1]Chemical Engineering and [2]Mechanical and Nuclear Engineering, Northwestern University, Evanston, IL 60201, U.S.A.

(*Received* 5 *May* 1986; *in revised form* 11 *December* 1986)

Abstract—Bubble size measurements by off-axis holography are reported for the first time in three-phase fluidized beds. The solid material was glass cylinders, with the liquid in one case having matching refractive index. Two different columns, 76 and 152 mm dia, were employed. An interpolative correlation was developed for the solid volume fraction of the bed as a function of liquid flux. A generalized dimensionless model was developed to predict the equilibrium bubble size in both fixed and fluidized beds.

1. INTRODUCTION

Interest in the fluid dynamics of three-phase fluidized beds has grown in recent years with the development of several chemical reaction processes requiring simultaneous gas–liquid–solid contacting, such as the catalytic hydroliquefaction of high-sulfur coal to synthetic fuels. In the H–coal process the hydrogenation takes place inside an ebullated-bed reactor in which a coal–oil slurry reacts with hydrogen gas while passing through a fluidized catalyst bed, usually cobalt molybdenate on alumina. Typical operating conditions are 400–450°C at about 20 MPa. Three-phase fluidized-bed reactors are also used in the methanation or Fischer–Tropsch conversion of coal-derived synthesis gases. In this case, the liquid phase does not participate in the chemical reactions, but is used to fluidize the catalyst bed while removing the large amount of heat generated during conversion.

If a gas–liquid diffusion step is slower than subsequent diffusion and reaction steps, the surface area separating these phases, as determined from the bubble size distribution within the bed, is influential in determining the reaction kinetics. Such measurements have not been available previously, making it difficult to scale up reactor design.

The present research deals with the measurement of bed expansion and the sizes of gas bubbles flowing cocurrently upward with a liquid through a fluidized solid bed, using off-axis holography. The advantage, as compared to ordinary photography, of this technique is that it allows measurement of the entire bubble size and location distribution within the bed at a single instant of time. Bubble self-shielding is also minimized. Bed expansion measurements were also made, leading to a new correlation which fits experimental data for both fixed and fluidized beds, as well as the intermediate transition region.

2. LITERATURE REVIEW

Most of the three-phase fluidization research which has been published to date deals with the measurement and prediction of the volume fractions of each phase for various flow conditions (Bhatia 1972; Dhanuka & Stepanek 1978; Kito *et al.* 1975; Michelsen & Ostergaard 1970; Bhaga & Weber 1972).

In many cases where the gas flow rate is low, the solids are almost totally supported by the flowing liquid, and variations in the gas flow rate result in negligible changes in the bed height. Under these conditions, the empirical correlation developed by Richardson & Zaki (1954) for

†Present address: Amoco Chemicals Corp., Naperville, Ill., U.S.A.
‡To whom all correspondence should be addressed.

particle suspensions in fluids can be used to relate the solid volume fraction, ϵ_s, to the liquid flux, j_L:

$$j_L = v_\infty (1 - \epsilon_s)^n. \quad [1]$$

Here v_∞ is the terminal velocity of a single solid particle falling through the liquid, ϵ_s is the volume fraction of particles and n is the Richardson–Zaki index, which generally has a value between 2.39 and 4.90.

Several models have been developed for predicting the volume fractions present in three-phase fluidization. Empirical models have been developed by Razumov *et al.* (1973) and Begovich & Watson (1978). Theoretical models have been presented by Darton & Harrison (1975) and Bhatia & Epstein (1974), using the drift-flux approach (Wallis 1969). Both models incorporate the wake volume which exists behind large bubbles as they flow through the bed, since the liquid in the wake region rises faster than the surrounding liquid. The Bhatia–Epstein model requires knowledge of the liquid wake/bubble volume ratio, as well as the concentration of solids within the wake. The Darton–Harrison model relies on only one parameter to characterize the wakes, assuming the wakes to be particle-free.

Massimilla *et al.* (1961), Page & Harrison (1972) and Rigby *et al.* (1970) found that the bubble size distribution reaches an equilibrium after flowing about 0.6 m through beds with particle diameters < 1 mm. Bubble diameters measured for these fine-particle beds generally were between 10 and 50 mm.

Lee & Buckley (1981) measured bubble sizes for beds of 2, 4 and 6 mm dia glass particles, using both water and an octanol solution with surface tension about half that of water. Large bubbles were observed with 2 mm dia particles, decreasing with increasing particle size. The octanol solution was found to stabilize much smaller bubbles than water. In this case bubble sizes again decreased as the particle size was increased from 2 to 4 mm, but a further increase to 6 mm resulted in little change in bubble size. In a similar study, Kim *et al.* (1972) reported a critical particle size of about 2.5 mm for the transition from bubble coalescence to bubble disintegration as the particle size is increased.

Bubble sizes reported by Bruce & Revel-Chion (1974) were measured for 2, 4, 6 and 8 mm dia solids. Although the initial height of the solid bed was only 0.32 m, so that an equilibrium bubble size was not achieved, an interesting phenomenon was observed. As in earlier studies, the bubble size was found to decrease with increasing particle size, but only up to a point. When the particle size was increased to 8 mm, the equilibrium bubble size was larger than it had been for 6 mm dia particles, indicating a reversal in the trend. Their work suggests that a minimum bubble size occurs when the solid particle diameter lies between 4 and 6 mm for an air–water–glass system. Vasalos *et al.* (1980) later reported that a minimum bubble size exists when the particle size is between 3 and 4 mm. Kim *et al.* (1975) found that the bubble size decreases with increasing particle size until a minimum bubble size is achieved, while the bubble size increases with increasing liquid viscosity.

3. EQUIPMENT AND PROCEDURE

Experiments were conducted in two different three-phase flow columns, allowing two different liquids to be used without having to completely dismantle and clean the equipment. The larger column had a diameter of 152 mm, while the smaller column had a diameter of 76 mm.

The larger column, used with a mixture of two organic solvents, is shown in figure 1. The vertical column was constructed of four 0.61 m long sections of flanged glass pipe. Carbon-steel spool pieces between the glass pipe sections provided access to the interior of the column via threaded pipe connectors. The liquid phase flowed from a holding tank through a filter into the column through a globe valve and a rotameter. After flowing upward through the column, the fluid mixture was separated into gas and liquid phases by a spiral entrainment separator. The liquid then flowed through an overflow cup, down a return line and back into the holding tank. The gas phase was simply vented to the atmosphere. A stainless-steel screen was spot-welded to the overflow cup to prevent the entrainment of solids out of the column. The smaller column had a similar design. Additional details are given by Peterson (1985).

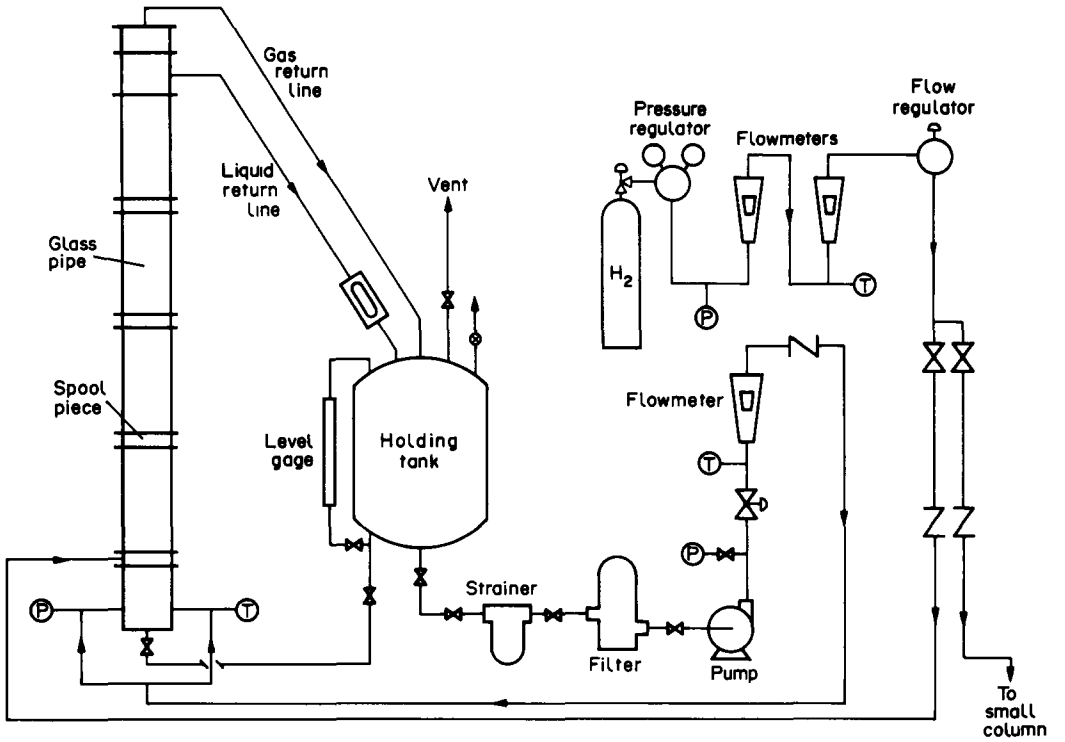

Figure 1. Schematic diagram of the large column and associated equipment.

The solid phase used in both columns consisted of Pyrex glass cylinders with average diameter 2.1 mm and length 5.7 mm. These particle dimensions closely simulated those of the catalyst particles used in the H–coal process (Schaefer *et al.* 1983). The liquid phase used in the larger column consisted of a mixture of two organic liquids whose refractive index matched that of the solid phase. These were Dowanol DPM (dipropylene glycol monomethyl ether) and diphenyl ether, which, when mixed 2:1, respectively, resulted in a refractive index of 1.474 n_D at 27°C. Bubble size measurements could also be obtained in the two-phase gas–liquid region just above the upper surface of the bed, making it possible to use distilled water as the liquid phase in the smaller column. It was thus possible to study the effect of surface tension on the bubble size.

Pressure drop measurements were obtained for both columns using a differential pressure transducer. A carrier demodulator unit connected to the transducer contained a bridge circuit for converting the coil inductance ratio to a D.C. output voltage. The transducer sensitivity was rated at 20 mV/V for full scale.

4. INSTRUMENTATION

The holographic equipment available in our laboratory (Stachniak 1979; Lee 1982) was modified to allow the construction of 3-D images of bubbles flowing within a three-phase fluidized bed.

Pulses of light from a Q-switched Nd:YAG laser were used to illuminate the test sections and form holograms for later analysis. The Nd:YAG laser used was a Quanta-Ray DCR-1 laser oscillator with "filled-in" optics capable of emitting up to 16 pulse/s at a wavelength of 1064 nm (i.r.). A Quanta-Ray HG-1 harmonic generator assembly with a Type II second harmonic SHG KD*P crystal was used to convert the pulses to a wavelength of 532 nm (green) with an energy of approx. 70 mJ/pulse and a pulse width of approx. 10 ns. By means of a Quanta-Ray ICE-1 temperature-controlled intracavity etalon and an ELN-1 electronic line-narrowing accessory, the linewidth of the output beam was reduced 100 times to $<0.02\,cm^{-1}$, thus producing a highly monochromatic light source with an increased coherence length. Figure 2 shows the basic equipment, while figure 3 illustrates the optics used to construct off-axis holograms. The laser beam was directed through a hole in the optical bench and returned to a horizontal position via mirrors.

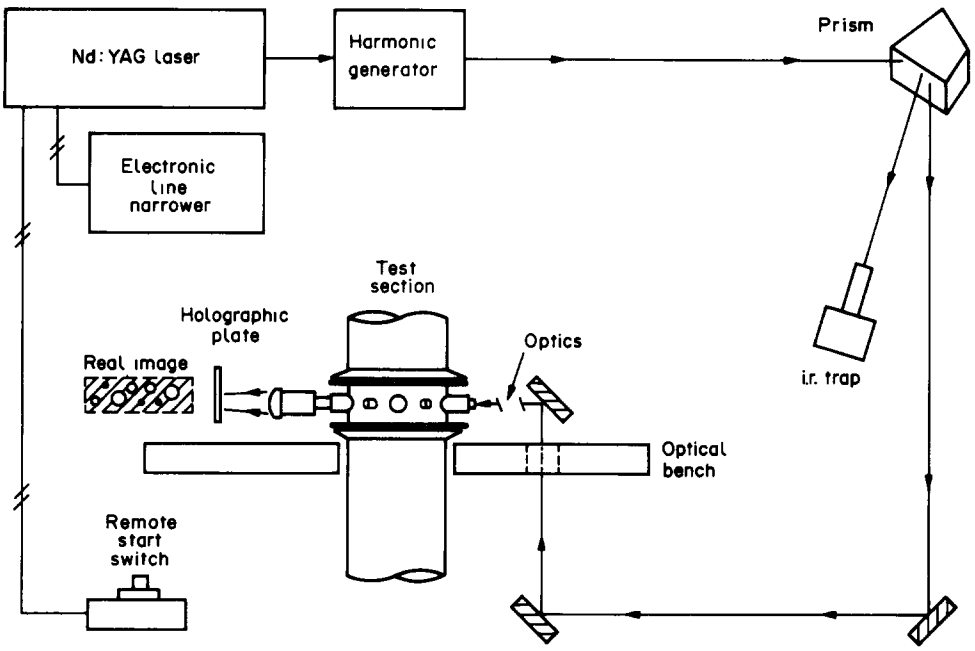

Figure 2. Equipment used to construct off-axis holograms.

The beam then passed through an iris diaphragm to adjust the beam diameter. Next, the beam was expanded to a diameter of approx. 50 mm via a plano-concave lens/off-axis parabolic mirror arrangement. The focal point of the lens (focal length of -73 mm) was made to coincide with that of the parabolic mirror, so that all light from the mirror was reflected in parallel rays. This laser

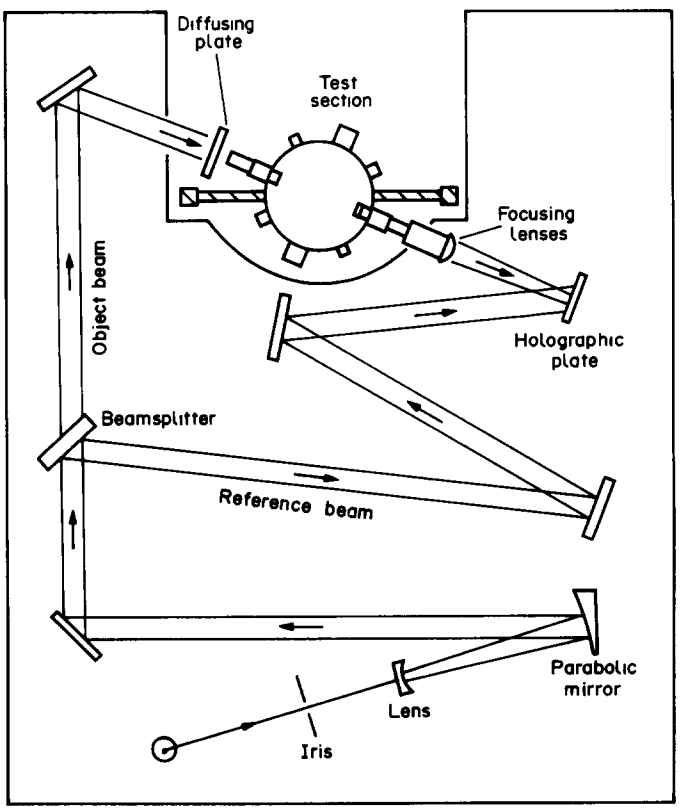

Figure 3. Optical bench.

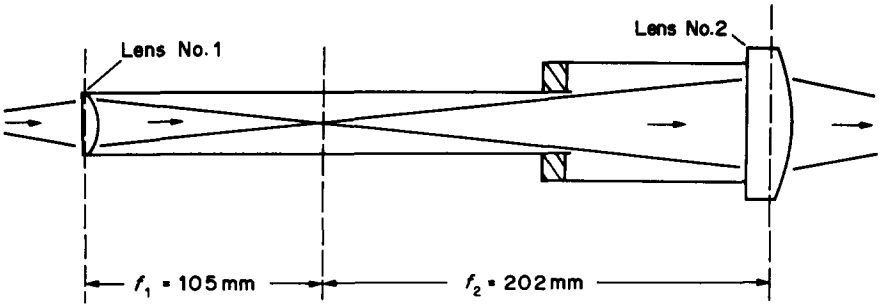

Figure 4. Focusing lenses.

beam was split into an object and a reference beam, using a 50:50 beamsplitter. The object beam passed through a diffusing plate and entered the test section through a 25.4 mm dia tube with a glass window on the end, positioned inside the column. The radial position of this tube was adjustable, allowing the viewing volume to be reduced so as to increase the intensity of transmitted light. The entire optical bench could be moved vertically, allowing different axial positions to be viewed.

Focusing lenses were used to produce an image of the viewing volume behind the holographic plate. Figure 4 shows the arrangement of the focusing lenses. The two lenses were separated by a distance equal to the sum of their focal lengths, causing the focused image to be magnified 1.9×. This configuration has relatively low spherical aberration and distortion. Finally, the focused light from the object beam was recombined with the off-axis reference beam in the plane of the holographic plate.

A new method of analyzing holograms was developed, making use of a video camera to view reconstructed holograms. The camera was interfaced with a digital electronic circuit designed (Peterson 1985) to record the horizontal and vertical positions of objects displayed on a video screen. This circuit was connected directly to a computer which calculated the bubble size and distributions. Some human judgment was required to choose bubbles which were in focus, but this allowed bubble sizes to be measured more accurately, and probably more cheaply, and in a shorter period of time than would be required for analysis of holographic data by scanning densitometers. The camera was fitted with a Fujinon CCTV lens (C10 × 16A, 1:1.8/16-160) which focused upon narrow "slices" from a holographic image at a magnification of approx. 10× and with a depth of field of about 5 mm. The video camera was mounted on a traversing mechanism capable of motion perpendicular to the focal plane. As the camera moved, different planes came into focus on the video screen, allowing bubble sizes to be measured at various depths into the hologram.

5. BED EXPANSION MEASUREMENTS

Bed expansion measurements were made for both the larger and smaller columns, which allowed the volume fraction of the solid phase to be calculated for various liquid fluxes. It was found that the bed expansion changed very little with varying gas flux, so that the bed expansion was effectively a function of the liquid flux only. Conditions ranged from a fixed bed at low liquid flow rates to a fully-fluidized state in which the beds expanded by as much as 180% in the larger column and up to 215% in the smaller column. Kim *et al.* (1975) and Epstein (1981) found that some three-phase fluidized beds expand when the gas flux is increased, some systems contract and some remain unchanged. Bed expansion was found to occur in systems of relatively large and/or heavy particles in non-viscous liquids where the wake volumes behind the bubbles were relatively small. In such cases, the majority of the liquid phase exists outside of the wake regions, so that an increase in the number of bubbles increases the liquid velocity around the solid particles, causing the bed to expand. Bed contraction was found to occur in systems of relatively small and/or light particles in viscous liquids. The generally accepted explanation for this contraction phenomenon is that these systems contain relatively large bubbles which have large wake volumes. The liquid present in the wake regions travels faster than the surrounding liquid, so that an increase in the number of bubbles would increase the amount of liquid in the wake region. Since this liquid, normally used

to fluidize the solid particles, is diverted to the solids-deficient wake regions the solid bed actually contracts. It was found (Kim *et al.* 1975; Epstein 1981) that the transition between bed expansion and bed contraction occurs at a particle size of about 3 mm in an air–water–glass system. Since the particles used in this study had a volume-equivalent spherical diameter of 3.35 mm, the observation that these beds were neither contracting nor expanding is in agreement with previous research.

It was observed that the bubbles in the two columns had relatively small wake volumes, with no solids inside the wakes. Assuming a homogeneous distribution of solids throughout the bed, it is possible to model the volume fraction of solids in the fully-fluidized beds using the Richardson–Zaki correlation [1]. Two such models based on a best fit to the fully-fluidized bed data are:

(a) For the 152 mm dia column using a 2:1 mixture of Dowanol DPM and diphenyl ether to fluidize a bed of 2 × 5 mm Pyrex cylinders,

$$j_L(\text{m/s}) = 0.186(1-\epsilon_s)^{2.55}. \quad [2]$$

(b) For the 7.6 mm dia column using distilled water to fluidize a bed of 2 × 5 mm Pyrex cylinders,

$$j_L(\text{m/s}) = 0.196(1-\epsilon_s)^{2.02}. \quad [3]$$

The Richardson–Zaki correlation requires only two parameters, the terminal velocity of a particle in the liquid phase and the Richardson–Zaki parameter, to describe the bed expansion when fully fluidized. These parameters can be estimated given the physical properties of the liquid and solid phases (Richardson & Zaki 1954). However, the Richardson–Zaki correlation does not fit the data for the transition region between a fixed bed and a fully-fluidized bed.

To overcome the limited usefulness of the Richardson–Zaki correlation a new model was developed to fit data taken in the fixed-bed region, the fully-fluidized region and the intermediate transition region:

$$(1-\epsilon_s) = (1-\epsilon_{s,\text{fixed}})\left[1+\left(\frac{j_L}{j_{L,\text{MF}}}\right)^{\frac{1}{mn}}\right]^m, \quad [4]$$

where $\epsilon_{s,\text{fixed}}$ is the fixed-bed solid volume fraction, $j_{L,\text{MF}}$ is the minimum fluidization flux, n is the Richardson–Zaki parameter and m is an additional empirical parameter. The minimum fluidization flux is here defined by the Richardson–Zaki correlation:

$$j_{L,MF} = v_\infty(1-\epsilon_{s,\text{fixed}})^n. \quad [5]$$

The parameter m can be determined from the solid volume fraction at the minimum fluidization flux:

$$m = \frac{\ln\left(\frac{1-\epsilon_{s,\text{MF}}}{1-\epsilon_{s,\text{fixed}}}\right)}{\ln 2}, \quad [6]$$

where $\epsilon_{s,\text{MF}}$ is the solid volume fraction at the minimum fluidization flux. The closer the parameter m is to zero, the sharper the transition becomes between a fixed and a fluidized bed.

Based on the bed expansion data for both columns the following models were constructed:

(a) For the 152 mm dia column using a 2:1 mixture of Dowanol DPM and diphenyl ether to fluidize a bed of 2 × 5 mm Pyrex cylinders,

$$(1-\epsilon_s) = 0.427[1+(46.9\,j_L)^{4.91}]^{0.08}. \quad [7]$$

(b) For the 76 mm dia column using distilled water to fluidize a bed of 2 × 5 mm Pyrex cylinders

$$(1-\epsilon_s) = 0.422[1+(29.2\,j_L)^{9.91}]^{0.05}. \quad [8]$$

Figures 5 and 6 show the bed expansion data, compared to the Richardson–Zaki correlations and to [7] and [8]. The new models allow the prediction of the solid volume fractions in the fixed-

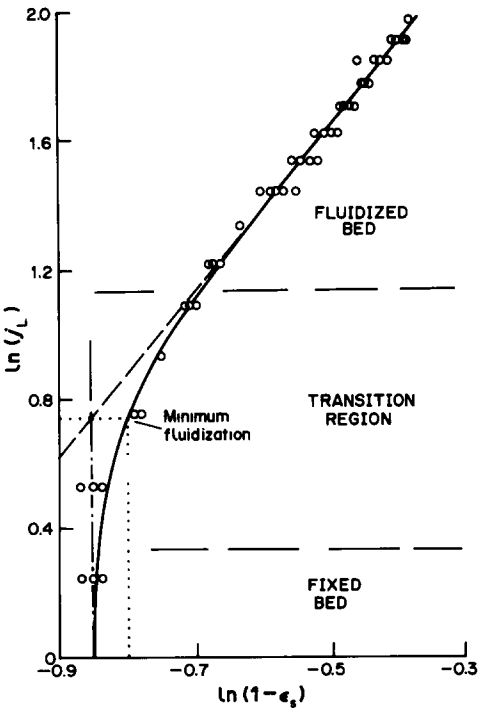

Figure 5. Bed expansion in the large column.

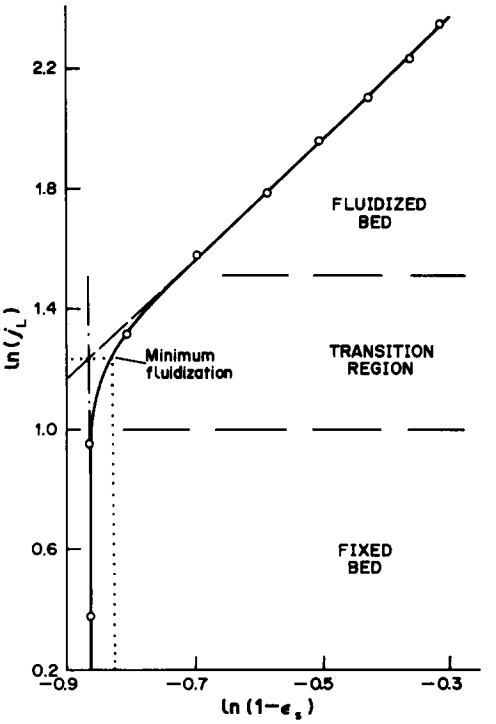

Figure 6. Bed expansion in the small column.

and fluidized-bed regimes as well as in the transition region. Equation [4] reduces to the Richardson–Zaki correlation for large liquid flux values and reduces to $\epsilon_s = \epsilon_{s,\text{fixed}}$ for a fixed bed.

6. BUBBLE BREAKUP AND COALESCENCE

One can expect that the bubbles will, on average, either coalesce or break up, depending upon their initial diameters compared to the solid particle diameter. For the case of large bubbles existing in bubble-coalescing beds, Henriksen & Ostergaard (1974) report that breakup is a result of Taylor instability of the bubble roofs. The bubble will not split if the solid particle is less than one-half the size of the minimum stable wavelength, $\lambda_{\min}$:

$$\lambda_{\min} = 2\pi\sqrt{\frac{\sigma}{\rho_L g}}, \qquad [9]$$

where σ is the surface tension and ρ_L is the liquid density. For smaller bubbles, breakup depends upon the Weber number and the energy dissipation rate (Ostergaard 1973; Hinze 1955), where the critical Weber number is defined in terms of the mean-square turbulent fluctuation velocity, $\overline{u^2}$ and the maximum stable bubble diameter, $d_{\max}$:

$$\text{We}_{\text{crit}} = \left(\frac{\overline{u^2} d_{\max}\rho_L}{\sigma}\right)_{\text{crit}}. \qquad [10]$$

Assuming homogeneous isotropic turbulence, the average of the squares of the velocity differences between two points separated by a distance d can be written as

$$\overline{u^2} = C_1(\xi d)^{\frac{2}{3}}, \qquad [11]$$

where ξ represents the energy dissipation rate per unit mass of liquid by small-scale eddies. Substituting [11] into [10] allows one to determine the maximum bubble size [$C_1 \cong 2.0$ (Batchelor 1951)]:

$$d_{\max} = \left(\frac{\text{We}_{\text{crit}}\sigma}{C_1\rho_L}\right)^{0.6}\xi^{-0.4}. \qquad [12]$$

Hinze found that the Sauter mean bubble diameter, d_{SM}, defined as the ratio of the volumetric mean diameter to the surface area mean diameter,

$$d_{SM} = \frac{\Sigma d_b^3}{\Sigma d_b^2}, \quad [13]$$

is approximately equal to one-half the maximum stable bubble diameter. By applying his theory to the experimental results of Clay (1940) for an agitated tank, Hinze arrived at the following model:

$$d_{95} = 0.725\left(\frac{\sigma}{\rho_L}\right)^{0.6} \xi^{-0.4}, \quad [14]$$

where d_{95} represents the bubble diameter below which 95% of the total gas volume exists.

The energy dissipation rate can be expressed as follows for a three-phase fluidized bed:

$$\xi = \frac{-\left(\frac{dp}{dz}\right)_F (j_L + j_G)}{\rho_L \epsilon_L}. \quad [15]$$

The frictional pressure gradient is given by

$$-\left(\frac{dp}{dz}\right)_F = -\frac{dP}{dz} - \rho_L g. \quad [16]$$

Upon equating the total pressure gradient to the hydrostatic head of the three phases present, one obtains

$$-\left(\frac{dp}{dz}\right)_F = g(\rho_s \epsilon_s + \rho_L \epsilon_L + \rho_G \epsilon_G - \rho_L \epsilon_L^* - \rho_G \epsilon_G^*), \quad [17]$$

where

$$\epsilon_L^* = \frac{\epsilon_L}{\epsilon_L + \epsilon_G} \quad [18]$$

and

$$\epsilon_G^* = 1 - \epsilon_L^*. \quad [19]$$

Therefore, neglecting the gas density compared to the densities of the solid and liquid phases, the energy dissipation rate per unit mass of liquid within a three-phase fluidized bed becomes

$$\xi = \frac{(\rho_s - \rho_L \epsilon_L^*)\epsilon_s g(j_L + j_G)}{\rho_L \epsilon_L}. \quad [20]$$

This allows the Weber number model to be applied to a three-phase fluidized bed.

A similar critical Weber number criterion for bubble breakup was developed by Lee *et al.* (1974) specifically for three-phase fluidization, but requires knowledge of the bubble velocities. No breakup is said to occur for

$$\frac{\rho_s u_b^2 d_p}{\sigma} \leqslant 3. \quad [21]$$

Meernik (1983) used an optical technique to measure bubble sizes in a three-phase fluidized bed. The following equilibrium bubble size model for 2, 3 and 5 mm dia glass spheres and 2 × 5 mm glass cylinders was obtained:

$$\frac{d_{SM}}{d_p} = 1.544\left[\frac{\sigma}{(\rho_s - \rho_L)d_p^2 g}\right] + 0.143. \quad [22]$$

It was also found that the mean bubble size in a three-phase fluidized bed reaches a minimum when the bed is near the point of minimum fluidization. This suggests the frictional pressure gradient may influence the bubble size since it reaches a maximum at the point of minimum fluidization.

Thomas (1981) extended the Hinze analysis of bubble breakup (Hinze 1955) to bubble coalescence in turbulent flows. It was found that bubbles will not coalesce unless their diameter is less than a critical diameter related to the critical film thickness, l, and the energy dissipation rate per unit mass, ξ. This gives rise to a minimum bubble diameter found in a turbulent flow:

$$d_{min} = 2.4\left(\frac{\sigma^2 l^2}{\mu_L \rho_L \xi}\right)^{\frac{1}{4}}. \quad [23]$$

This result has been shown to be valid for experiments in which the dominant factor determining droplet size was not breakup, but the prevention of coalescence due to turbulence.

Koide *et al.* (1968) measured the size of bubbles generated from a porous plate and found that the type of liquid used plays an important role in determining the bubble size distribution. Pure liquids resulted in bubbles which coalesced easily, with the size of generated bubbles changing with the gas flow rate. Mixtures of organic solvents where one solvent acts as a surfactant, however, resulted in a narrower size distribution, with little change occurring as the gas flow rate was changed.

7. RATE OF BUBBLE BREAKUP

Bubble sizes were measured at various distances from the gas spargers where bubbles first entered the fluidized beds. This allowed the rate of bubble breakup to be determined, as the relatively large bubbles injected into the beds were broken down while they flowed upward. From these data an equilibrium value of the Sauter mean bubble diameter was estimated for each of the fluidized beds examined.

Experiments were conducted using two different liquid flow rates in each of the two columns. These flow rates were chosen so that the beds were fully fluidized and operated at identical solid volume fractions of 0.44 and 0.33. Two different gas flow rates were chosen for the experiments run in the larger column, but this had little influence on the bubble size as long as the system was operated within the regime of bubble flow. Because of this observation, only one gas flow rate was used in the smaller column. This value was chosen so the gas flux would be between those used in the larger column. Table 1 lists the various conditions for the experiments used to measure the rate of bubble breakup.

A 2:1 mixture of Dowanol DPM and diphenyl ether was used in the 152 mm dia column to fluidize the solid bed. This organic mixture, chosen to match the refractive index of the solids, was found to inhibit bubble coalescence, so that once large bubbles were broken into smaller bubbles they did not readily coalesce. This phenomenon is attributed to the presence of the diphenyl ether, which was found to act as a mild surfactant for the Dowanol DPM, preferentially orienting itself on the gas–liquid interface so as to set up a net dipole charge. This charge would then cause small bubbles to repel one another, rather than coalesce.

Because of this slow rate of coalescence it was possible to measure bubble sizes above the top of the bed in order to determine the bubble size which existed at the top of the bed. By varying the total volume of solids in the bed it was possible to change the amount of bubble breakup which occurred. Large bubbles were introduced at the base of the column and flowed upward, breaking up along the way. After emerging from the top of the bed, no further breakup or coalescence occurred while the bubbles flowed upward to the height at which they were measured.

Table 1. Experimental conditions for measurement of the rate of bubble breakup

Liquid	Column diameter (mm)	j_L(mm/s)	j_G(mm/s)	ϵ_s
DPM + DE	152	42.5	1.4	0.44
DPM + DE	152	42.5	4.6	0.44
DPM + DE	152	68.0	1.4	0.33
DPM + DE	152	68.0	4.6	0.33
Water	76	59.8	2.4	0.44
Water	76	89.0	2.4	0.33

DPM + DE = 66% Dowanol DPM + 34% diphenyl ether.

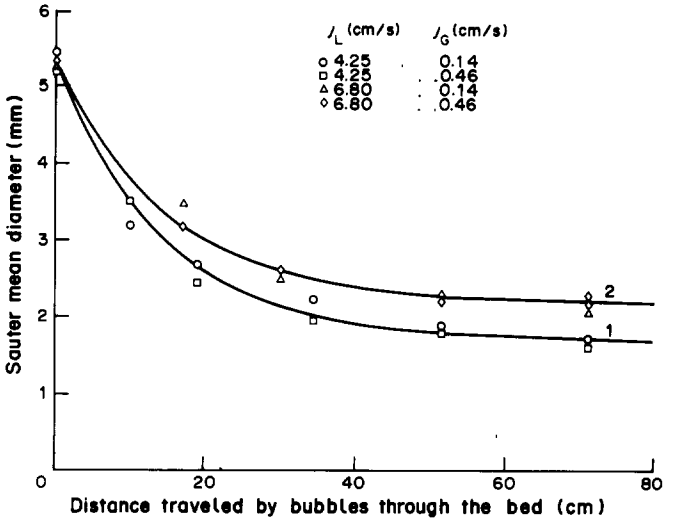

Figure 7. Plot of the Sauter mean diameter vs the distance traveled by the bubbles through the bed (large column): 1, [25]; 2, [26].

By changing the total volume of solids in the column the top of the bed was lowered or raised, effectively allowing bubbles to be measured at different distances from the gas inlet.

In order to verify that the bubble size did not change very much once the bubbles emerged from the top of the bed, bubbles were measured at two heights of 20 and 730 mm above the top of the bed, while operating under the same conditions ($j_L = 29.8$ mm/s and $j_G = 1.4$ mm/s). The Sauter mean bubble diameters obtained from these runs were 15.7 and 16.0 mm, respectively. These values were close enough to conclude that no significant change in bubble size occurred in the larger column once the bubbles left the fluidized bed and flowed through the liquid.

The results of bubble size measurements for the larger column, illustrated in figure 7, show that a change in the gas flux had little effect on the stable bubble size. However, an increase in the liquid flux increased the bubble sizes when the bed was fully fluidized. Assuming exponential decay for the Sauter mean bubble diameter, a simple model is given by

$$d_{SM} = (d_{SM,0} - d_{SM,E})\exp\left(-\frac{z}{b}\right) + d_{SM,E}, \qquad [24]$$

where

$d_{SM,0}$ = initial Sauter mean bubble diameter entering the bed (mm),
$d_{SM,E}$ = equilibrium Sauter mean bubble diameter (mm),
z = vertical distance from gas entrance (mm)

and

b = rate constant for bubble breakup.

As shown in figure 7, the data were then correlated for the two liquid fluxes studied by:

(a) for $j_L = 42.5$ mm/s,

$$d_{SM} = 3.61\exp\left(-\frac{z}{144}\right) + 1.69; \qquad [25]$$

and

(b) for $j_L = 68.0$ mm/s,

$$d_{SM} = 3.12\exp\left(-\frac{z}{151}\right) + 2.18. \qquad [26]$$

Distilled water was used in the smaller column with a movable gas sparger to allow different depths of submergence. The bubble size measurements in the smaller column (figure 8) show similar

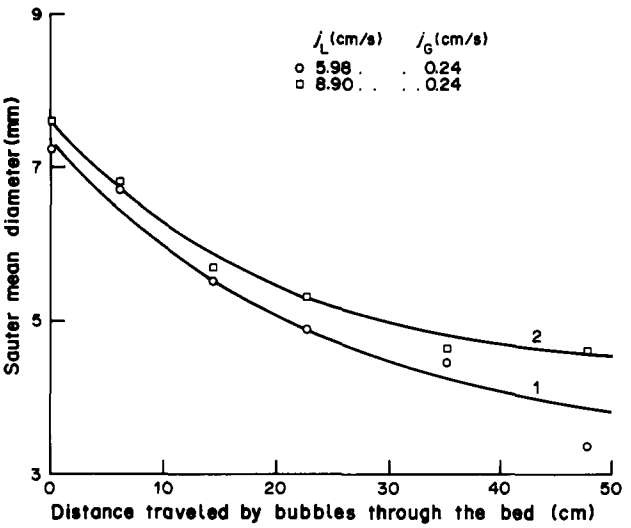

Figure 8. Plot of the Sauter mean diameter vs the distance traveled by the bubbles through the bed (small column): 1, [27], 2, [28]).

breakup, but leading to larger bubbles. Using the exponential decay model, the correlations were:

(a) for $j_L = 59.8$ mm/s,

$$d_{SM} = 4.03 \exp\left(-\frac{z}{246}\right) + 3.30; \qquad [27]$$

and

(b) for $j_L = 89.0$ mm/s,

$$d_{SM} = 3.30 \exp\left(-\frac{z}{189}\right) + 4.32. \qquad [28]$$

Using different liquid flow rates in the larger column, bubble measurements were made with the fixed bed, fully-fluidized bed and for the transition region between the two. Figure 9 illustrates the change in the Sauter mean bubble diameter with liquid flux and, consequently, the frictional pressure gradient. It is seen that the bubble size varies inversely with the frictional pressure gradient.

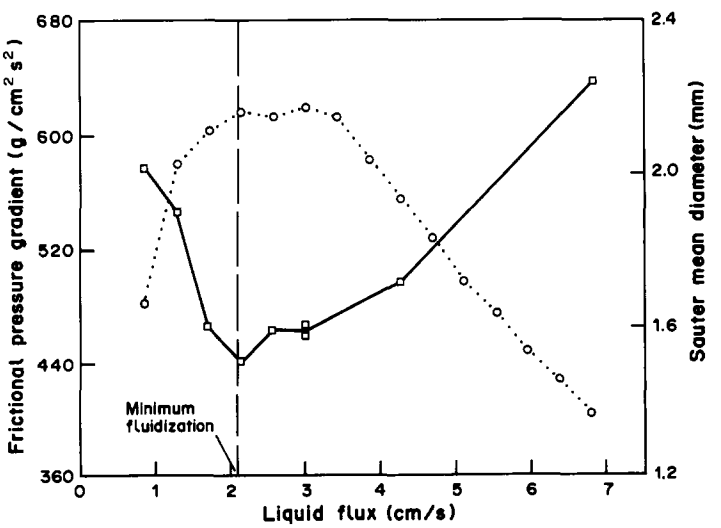

Figure 9. Plot of the frictional pressure gradient (○) and the Sauter mean diameter (□) vs liquid flux (large column).

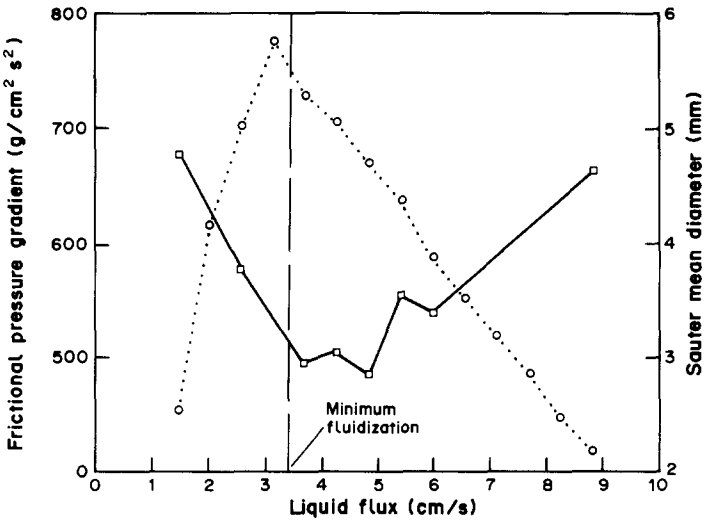

Figure 10. Plot of the frictional pressure gradient (○) and the Sauter mean diameter (□) vs liquid flux (small column).

A minimum value of the average bubble size was found to occur near the point of minimum fluidization, in agreement with observations by Meernik (1983). The Sauter mean bubble diameter decreased as the liquid flux increased when the bed was not fluidized. When the bed became fluidized this trend was reversed and the bubble size started to increase as the liquid flux was increased.

The results with water in the smaller column (figure 10) were similar to those with organics in the larger column, but the average bubble sizes in water were larger, as expected. Once again it was observed that the average bubble size decreased as the liquid flux increased when the bed was not fluidized and the minimum Sauter mean bubble diameter was found to occur near the point of minimum fluidization.

By assuming a volume-equivalent spherical diameter (3.35 mm) for the 2.1 × 5.7 mm Pyrex cylinders used in this study, the following correlation for the dimensionless equilibrium Sauter mean bubble diameter was constructed:

$$\frac{d_{SM,E}}{d_p} = 0.918\left[\frac{\sigma}{-\left(\frac{dp}{dz}\right)_F d_p^2}\right]^{0.8}. \quad [29]$$

Equation [29] can be used for either a fixed-bed or a fluidized-bed system. When the bed is fluidized, the frictional pressure gradient is given by

$$\frac{d_{SM,E}}{d_p} = 0.918\left[\frac{\sigma}{(\rho_s - \rho_L \epsilon_L^*)\epsilon_s g d_p^2}\right]^{0.8}. \quad [30]$$

Figures 11 and 12 show the Sauter mean bubble diameter plotted vs the liquid flux for the organic liquid mixture and distilled water. Both the experimental values and the values predicted by [29] are shown. The model seems to predict the equilibrium bubble size quite accurately when the bed is fluidized and also predicts the occurrence of a minimum bubble size near the point of minimum fluidization.

For low values of the liquid flux when the bed is not fluidized, the model predicts equilibrium bubble sizes which are smaller than the bubble sizes measured at a single downstream position. The bubbles were assumed to have achieved their equilibrium size, but in reality may have been larger. It would be necessary to make several measurements, and then extrapolate to infinity in order more accurately to determine the equilibrium bubble size experimentally for a fixed-bed system. If nothing else, the model given in [29] at least gives approximate values of the equilibrium bubble size in the fixed-bed region.

It should be noted that [29] fits the experimental data from this study much better than any other model previously proposed. The correlation due to Meernik, [22], does not predict any change in

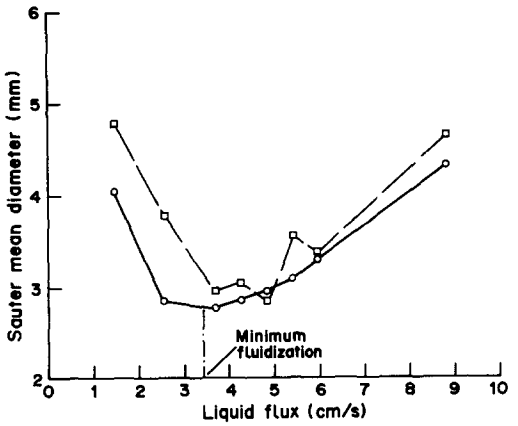

Figure 11. Plot of measured (□) and predicted values (○, [29]) of the Sauter mean diameter vs liquid flux (large column).

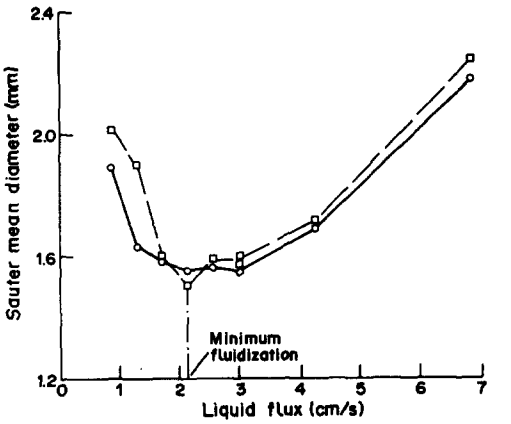

Figure 12. Plot of measured (□) and predicted values (○, [12]) of the Sauter mean diameter vs liquid flux (small column).

the equilibrium bubble size as the extent of fluidization changes. The Weber number model, [14]–[20], is based upon the energy dissipation rate in the bed, and was found to yield values of the equilibrium bubble size which were much worse than those obtained from [29]. However, all of the experiments conducted during this study were based upon a single solid particle size. Therefore, [29] was tested against data from Meernik (1983) and from Lee & Buckley (1981), who measured bubble sizes in three-phase fluidized beds for different solid particles and liquids. Since all of these data were gathered for fluidized beds, [30] was used to predict the equilibrium Sauter mean bubble diameter for each case. From figure 13 it is clear that the dimensionless model accurately predicts the equilibrium Sauter mean bubble diameter for the cases shown. The largest deviations from the predicted values occur for the data gathered by Meernik (1983). However, it should be noted that Meernik only measured bubbles at a single elevation and assumed the bubbles had achieved equilibrium. Also, his light-probe technique used to measure bubble diameters was not able to measure larger, non-spherical bubbles as accurately as smaller, spherical bubbles. Since the Sauter mean is more sensitive to deviations in the large-diameter values than in the smaller ones, this could have led to equilibrium Sauter mean bubble diameters which were underestimated.

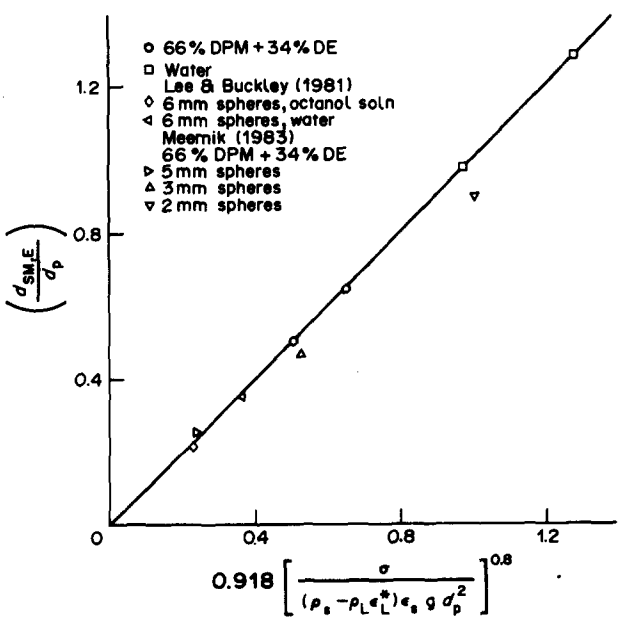

Figure 13. Plot of the dimensionless equilibrium Sauter mean bubble diameter vs [30].

Acknowledgements—This work was supported by a subcontract with Amoco Oil Co. on Contract DE-AC22-80PC-30026 with the Department of Energy. The help in designing and constructing the 152 mm dia column and circulating system of R. J. Schaefer and D. N. Rundell of the Amoco Research & Development Department (Naperville, Ill.) is acknowledged with thanks. Professor M. C. Yuen (Department of Mechanical and Nuclear Engineering, Northwestern University, Evanston, Ill.) provided helpful comments, and in addition supervised the work of P. R. Meernik (1983), who worked together with the first author to get the equipment functioning. We wish also to acknowledge with thanks the work of Mr G. Kettnocker, who was supported by a grant from the F.R.G., and who built the small column and took some of the data.

REFERENCES

BATCHELOR, G. K. 1951 Fluctuations in isotropic turbulence. *Proc. Camb. phil. Soc.* **47,** 359–374.

BEGOVICH, J. M. & WATSON, J. S. 1978 Hydrodynamic characteristics of three-phase fluidized beds. In *Fluidization; Proc. 2nd Engng Fdn Conf.* (Edited by DAVIDSON, J. F. & KEAIRNS, D. L.), pp. 190–195. Cambridge Univ. Press, Cambs.

BHAGA, D. & WEBER, M. E. 1972 Holdup in vertical two and three phase flow. *Can. J. chem. Engng* **5,** 323–336.

BHATIA, V. K. 1972 Holdup studies in three phase fluidized beds and related systems. Ph.D. Dissertation, Univ. of British Columbia, Vancouver, B.C.

BHATIA, V. K. & EPSTEIN, N. 1974 Three-phase fluidization: a generalized wake model. In *Proc. Int. Symp. on Fluidization and Its Applications*, Toulouse, France, pp. 380–392. Cepadues-Editions.

BRUCE, P. N. & REVEL-CHION, L. 1974 Bed porosity in three-phase fluidization. *Powder Technol.* **10,** 243–249.

CLAY, P. H. 1940 The mechanism of emulsion formation in turbulent flow. *K. Akademie Van Wetenschappen Amsterdaem, Section of Sciences Proc.* **43,** 852–865 (experimental part); 979–990 (theoretical part & discussion).

DARTON, R. C. & HARRISON, D. 1975 Gas and liquid hold-up in three-phase fluidization. *Chem. Engng Sci.* **30,** 581–586.

DHANUKA, V. R. & STEPANEK, J. B. 1978 Gas and liquid hold-up and pressure drop measurements in a three-phase fluidized bed. In *Fluidization; Proc. 2nd Engng Fdn Conf.* (Edited by DAVIDSON, J. F. & KEAIRNS, D. L.), pp. 179–189. Cambridge Univ. Press, Cambs.

EPSTEIN, N. 1981 Three-phase fluidization: some knowledge gaps. *Can. J. chem. Engng* **59,** 649–657.

HENRIKSEN, H. K. & OSTERGAARD, K. 1974 On the mechanism of breakup of large bubbles in liquids and three-phase fluidized beds. *Chem. Engng Sci.* **29,** 626–629.

HINZE, J. O. 1955 Fundamentals of the hydrodynamic mechanism of splitting in dispersion processes. *AIChE Jl* **3,** 289–295.

KIM, S. D., BAKER, C. G. J. & BERGOUGNOU, M. A. 1972 Hold-up and axial mixing characteristics of two and three phase fluidized beds. *Can. J. chem. Engng* **50,** 695–701.

KIM, S. D., BAKER, C. G. J. & BERGOUGNOU, M. A. 1975 Phase hold-up characteristics of three phase fluidized beds. *Can. J. chem. Engng* **53,** 134–139.

KITO, M., SHIMADA, M., SAKAI, T., SUGIYAMA, S. & WEN, C. Y. 1975 Performance of turbulent bed contactor: gas holdup and interfacial area under liquid stagnant flow. In *Fluidization Technology*, Vol. 1; *Proc. Int. Fluidization Conf.* McGraw-Hill, New York.

KOIDE, K., KATO, S., TANAKA, Y. & KUBOTA, H. 1968 Bubbles generated from porous plate. *J. chem. Engng Japan* **1,** 51–56.

LEE, J. C. & BUCKLEY, P. S. 1981 Fluid mechanics and aeration characteristics of fluidized beds. In *Biological Fluidized Bed Treatment of Water and Wastewater* (Edited by COOPER, P. F. & ATKINSON, B.), pp. 62–74. Halsted Press, New York.

LEE, J. C., SHERRARD, A. J. & BUCKLEY, P. S. 1974 Optimum particle size in three-phase fluidized bed reactors. In *La Fluidization et ses Applications*, pp. 407–416. Societe Chimie Industrielle, Toulouse.

LEE, S. Y. 1982 Behavior of water spray injected into air/steam environment. Ph.D. Dissertation, Mechanical and Nuclear Engineering Dept, Northwestern Univ., Evanston, Ill.

MASSIMILLA, L., SOLIMANDO, A. & SQUILLACE, E. 1961 Gas dispersion in solid–liquid fluidized beds. *Br. chem. Engng* **6,** 232–239.

MEERNIK, P. R. 1983 An optical technique for the determination of bubble size distributions and its application to a three-phase fluidized bed system. Ph.D. Dissertation, Mechanical and Nuclear Engineering Dept, Northwestern Univ., Evanston, Ill.

MICHELSEN, M. L. & OSTERGAARD, K. 1970 Hold-up and fluid mixing in gas–liquid fluidized beds. *Chem. engng J.* **1**, 37–46.

OSTERGAARD, K. 1973 Flow phenomena of three-phase (gas–liquid–solid) fluidized beds. *AIChE Symp. Ser.* **69** (128), 28–29.

PAGE, R. E. & HARRISON, D. 1972 The size distribution of gas bubbles leaving a three-phase fluidized bed. *Powder Technol.* **6**, 245–249.

PETERSON, D. A. 1985 Bubble breakup and coalescence in a three-phase fluidized bed. Ph.D. Dissertation, Chemical Engineering Dept, Northwestern Univ., Evanston, Ill.

RAZUMOV, I. M., MANSHILIN, V. V. & NEMETS, L. L. 1973 The structure of three-phase fluidized beds. *Int. chem. Engng* **13**, 57–61.

RICHARDSON, J. F. & ZAKI, W. N. 1954 Sedimentation and fluidization. *Trans. Instn chem. Engrs* **32**, 35–53.

RIGBY, G. R., VAN BLOCKLAND, G. P., PARK W. H. & CAPES, C. E. 1970 Properties of bubbles in three phase fluidized beds as measured by an electroresistivity probe. *Chem. Engng Sci.* **25**, 1729–1741.

SCHAEFER, R. J., RUNDELL, D. N. & SHOU, J. K. 1983 Study of ebullated-bed fluid dynamics. Final Progress Report (USDOE Contract No. DE-AC22-80PC-30026), Amoco Oil Co., Naperville, Ill.

STACHNIAK, R. E. 1979 Pulsed holography of two phase air and water mixtures using a Q-switched Nd:YAG laser. M.S. Thesis, Northwestern Univ., Evanston, Ill.

THOMAS, R. M. 1981 Bubble coalescence in turbulent flows. *Int. J. Multiphase Flow* **7**, 709–717.

VASALOS, I. A., BILD, E. M., RUNDELL, D. N. & TATERSON, D. F. 1980 H–coal fluid dynamics. Final Technical Progress Report (USDOE Contract No. DE-AC05-77ET-10149), Amoco Oil Co., Naperville, Ill.

WALLIS, G. B. 1969 *One Dimensional Two-phase Flow*. McGraw-Hill, New York.